Available online at www.sciencedirect.com
SCIENCE DIRECT®
Marine Geology 199 (2003) 83–100
MARINE GEOLOGY
INTERNATIONAL JOURNAL OF MARINE GEOLOGY, GEOCHEMISTRY AND GEOPHYSICS
www.elsevier.com/locate/margeo

Event-based stratigraphic simulation of wave-dominated shallow-marine environments

Joep E.A. Storms *

Department of Applied Earth Sciences, Delft University of Technology, Mijnbouwstraat 120, 2628 RX Delft, The Netherlands

Received 20 November 2001; received in revised form 3 February 2003; accepted 12 May 2003

Abstract

The presence of event beds in the shallow-marine stratigraphic record indicates formation is governed by high magnitude–low frequency processes rather than low magnitude–high frequency processes. In this paper, a 2-D multiple grain-size process-response model (BARSIM) is presented, which uses event deposition to simulate stratigraphic response to changes in sea level and sediment supply. BARSIM uses variable time steps to simulate individual storm (event) and fair-weather periods. Deposition during storm conditions solely consists of reworked shoreface sediment, while fair-weather deposits consist of reworked shoreface sediment combined with sediment supplied by littoral drift and suspension. Simulations using variations in sea level, sediment supply (both amount and grain-size) and wave-height regime result in distinct depositional patterns, stratal geometry and bed characteristics. Model results indicate that both wave-height regime and grain-size of supplied sediment have considerable effect on shoreface morphology and stratal characteristics. Unraveling coastal evolution from the shallow-marine stratigraphic record may therefore be more difficult than previously assumed, as both variables are expected to vary over geologic time scales.

Keywords: storm bed; wave climate; numerical modelling; sea-level change; sediment supply

1. Introduction

A wave-dominated shallow-marine system consists of an assemblage of depositional environments (Swift et al., 1991; Thorne and Swift, 1991), comprising coastal plain, lagoon, washover, shoreface (proximal and distal), and shelf. Throughout the geological past, shifting of these assemblages gave rise to different types of shallow-marine deposits while sea level and sediment supply constantly changed. The stratigraphic signature of these deposits contains important information about the palaeoconditions of individual depositional environments during the time of deposition. Understanding these deposits is relevant not only from a scientific point of view, but also for hydrocarbon exploration and environmental issues, as sea level most likely will rise in the years to come.

Transport of sediments in shallow-marine environments is governed by local hydraulic regimes, which can be described on many temporal scales

* Fax: +31-15-2781189.
E-mail address: j.e.a.storms@ta.tudelft.nl (J.E.A. Storms).

0025-3227/03/$ – see front matter © 2003 Elsevier Science B.V. All rights reserved.
doi:10.1016/S0025-3227(03)00144-0

ranging from the passage of a single wave (seconds to minutes) to a changing storm climate (millennia). Short-term sediment dispersal due to wave-generated oscillatory currents results in typical sedimentary structures related to water depth (Madsen, 1991; Myrow and Southard, 1996). A series of waves approaching the coast during high-energy conditions (i.e. a storm event) can generate shore-perpendicular and shore-parallel currents (e.g. Field and Roy, 1984; Cacchione et al., 1984, Snedden et al., 1988) which cause resuspension of sediments at the sea bottom. As such, sediments from the upper shoreface and the foreshore are picked up (Swift et al., 1991) and transported, resulting in a characteristic event stratification consisting of individual event beds (Kumar and Sanders, 1976; Lavelle et al., 1978; Lee et al., 1998; Swift et al., 1991, Drake, 1999; Niedoroda et al., 1984). This implies that the shallow-marine stratigraphic record is built predominantly by high magnitude–low frequency processes rather than low magnitude–high frequency processes. Event beds are sharp based and have a burrowed or diffuse upper contact (Kreisa, 1981). The base consists of a coarse-grained lag deposit that formed during the storm climax. As the storm passes, current velocity decreases and successively finer grains are deposited to form centimetre-scaled fining upward successions. The upper parts of event beds are usually bioturbated or eroded during later events (Wiberg, 2000). Research on event beds has shown that sedimentation rate and completeness of the stratigraphic record are highly variable in time and space (e.g. Gretener, 1967; Kumar and Sanders, 1976; Sadler, 1981; Dott, 1983; Crowley, 1984; Schwarzacher, 2000; Tipper, 2000). Variables controlling event-bed formation are the sequence of events and time-averaged value of fluid power expended by waves and bottom currents, the grain-size of the available sediment and the sedimentation rate (Niedoroda et al., 1989). Preservation of individual event beds will vary along the shoreface as a function of wave erosion and biogenous mixing rate (Wheatcroft, 1990). Storm beds may be interbedded with finer-grained deposits that formed under less energetic fair-weather conditions (Battacharyya et al., 1980; Kreisa, 1981; Aigner, 1985).

Numerical models can unravel shallow-marine deposits as they simulate the geomorphic response to changes in sea level and sediment supply. Modelling provides a way to simulate coastal behaviour in the absence of sufficiently long observational time-series. There is a wide diversity of forward numerical models for shallow-marine depositional environments available, each of which is built for specific goals (e.g. Niedoroda et al., 1989; Wheatcroft, 1990; Niedoroda et al., 1995; Zhang et al., 1997; Carey et al., 1999; Cowell et al., 1999a; Steckler, 1999; Zhang et al., 1999; Cookman and Flemmings, 2001; Harris and Wiberg, 2001; Li and Amos, 2001; Syvitski and Hutton, 2001; Storms et al., 2002). A well-documented overview of various approaches of forward numerical models can be found in Paola (2000) and will not be discussed here.

This paper discusses a 2-D process-response model (Storms et al., 2002) that has been adapted to simulate coastal evolution over geologic time scales on the basis of event deposition. The revised model (BARSIM) presented here uses a stochastic component to describe event magnitude and frequency and discriminates between storm and fair-weather conditions. It provides the opportunity to evaluate small-scale stratigraphic variability (e.g. grain-size, bed thickness, preservation potential) within the context of large-scale transgressive and regressive sediment bodies.

2. Process-response model

2.1. Model algorithms

BARSIM is a 2-D process-response model that simulates wave-dominated coastal response to external forcing on a geological time scale (Storms et al., 2002). BARSIM is based on a mass conservation principle:

$$\frac{\partial H}{\partial t} = -\frac{\partial F}{\partial x} + T \tag{1}$$

where t is time [T], x is horizontal distance [L], H is topographic elevation relative to a constant reference level [L], F is sediment flux [L^2T^{-1}] and T is rate of subsidence due to the combined

effects of compaction, loading, and vertical movements of the basin floor [LT^{-1}].

The spatial derivative of the sediment flux is defined as the difference between rates of erosion and rates of deposition at any given time and location:

$$\frac{\partial F}{\partial x} = E(x,t) - S(x,t) \quad (2)$$

where $E(x,t)$ is the rate of erosion [LT^{-1}] and $S(x,t)$ is the rate of deposition [LT^{-1}].

Instead of calculating all fluxes for consecutive cells in the downstream direction, we make use of the fact that the net effects of erosion and deposition in the coastal zone allow us to model the changes during each time step in three phases (Fig. 1):

Phase 1. The total flux available for deposition is calculated by summation of the erosion fluxes in the entire shoreface erosion window, which extends from the barrier coast to the wave base. The total deposition flux is calculated as the sum of the total erosion flux and the influx of additional sediment by longshore drift.

Phase 2. Backbarrier deposition.

Phase 3. Shoreface–shelf deposition. A constant fall-out rate is added to the deposition flux.

The coastline serves as an internal boundary condition in all three phases. This method of solution is not only more realistic from a geological standpoint, it is also computationally more efficient and numerically stable.

2.1.1. Erosion (Phase 1)

We define the rate of erosion as:

$$E(x,t) = c_e \cdot c_d(t) \cdot c_w(t) \cdot G(x,t) \quad (3)$$

where $G(x,t)$ is the local erosion efficiency [−]:

$$G(x,t) = \left(\frac{H(x,t) - H_w(t)}{H_s(t) - H_w(t)}\right)^m \text{ for } x_s(t) < x < x_w(t) \quad (4)$$

$$G(x,t) = 0 \text{ for } x \le x_s(t) \text{ and } x \ge x_w(t) \quad (5)$$

Location $x_s(t)$ corresponds to the coastline, which is defined by the intersection of sea level $H_s(t)$ and the topographic profile (Fig. 1). Erosion is limited to a shoreface erosion window defined by the spatial domain between locations $x_s(t)$ and $x_w(t)$, and outside of this domain, $E(x,t)$ is taken to be zero. The topographic elevation at $x_s(t)$ is defined as $H_s(t)$. Location $x_w(t)$ is defined by the intersection of the wave base $H_w(t)$ and the topographic profile. The wave base $H_w(t)$ is defined by: $H_w(t) = H_s(t) - z_w(t)$, where $z_w(t)$ is the depth

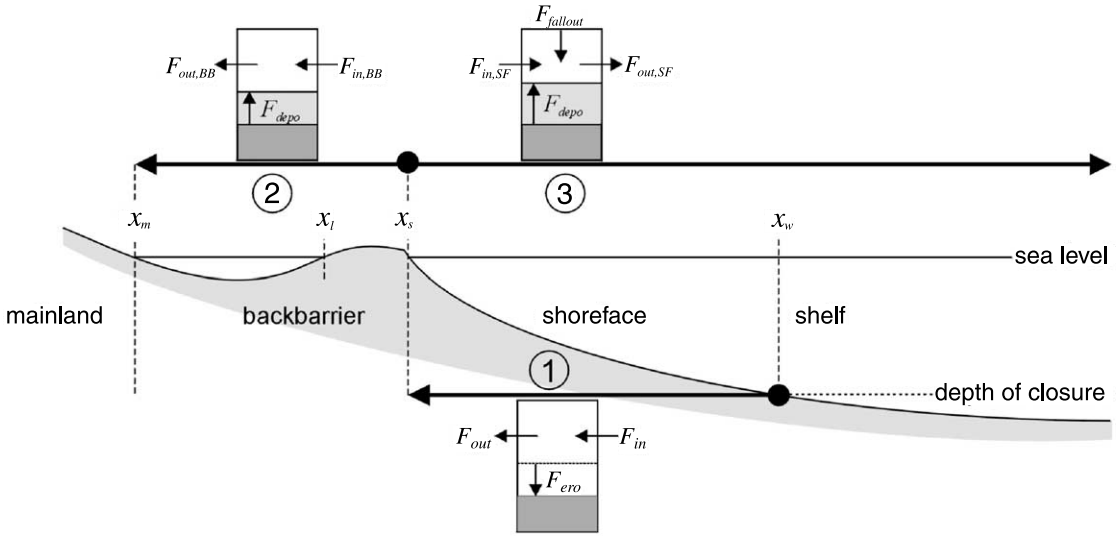

Fig. 1. Schematic cross section of the sediment fluxes and model domains used in BARSIM. Three phases of sediment dispersal can be distinguished: shoreface erosion, deposition in the backbarrier (if present) and shoreface–shelf deposition. See text for explanation.

of closure [L], which is defined as the maximum water depth for waves to affect the sea bottom (Cowell et al., 1999b). The depth of closure is chosen as a function of wave height: $z_w(t) = c_c w(t)$, in which c_c is a constant (Table 1). The above definitions allow us to formulate local erosion efficiency, with values ranging from unity in the vicinity of the coastline to zero at the storm wave base. Constant m [−] represents the dependence of erosion rate on water depth (Table 1).

The erosion efficiency rate c_e [LT^{-1}] is independent of the properties of the unconsolidated substrate (Table 1). The parameter $c_d(t)$ [−] reflects the local dissipation constant.

$$c_d(t) = 1 + \frac{\alpha_s(t) - \alpha_r}{\alpha_r} \quad (6)$$

where $\alpha_s(t)$ is the mean gradient of the shoreface and α_r [−] (Table 1) is a value for a reference shoreface gradient. A shallow shoreface gradient, relative to α_r, leads to wave-energy dissipation. This decreases the erosion potential between the wave base and the coastline. Parameter $c_w(t)$ [−] corrects for temporal variation in wave energy:

$$c_w(t) = \frac{w(t)}{w_{fw}} \quad (7)$$

where w_{fw}[L] and $w(t)$ [L] are the fair-weather and the actual wave height (Table 1). Large waves increase the erosion potential.

The total sediment flux available for deposition is equal to:

Table 1
Values and units of parameters used in BARSIM

Parameter	Value	Unit
c_c	7	–
m	3	–
c_e	2.5	m yr^{-1}
α_{ref}	0.005	–
w_{fw}	4	m
F_{add}	0–40	m^2 yr^{-1}
k	0–0.002	m yr^{-1}
D_{ref}	0.125	mm
c_g	7.5–17.5	–
t_{min}	1–40	yr
a_1	1–5	–
a_2	1–5	–

See text for further explanation of the parameters.

$$F_t(t, D) = \sum_{x=x_s}^{x=x_w} [E(x,t)\cdot(x_s(t) - x_w(t))] + F_{add}(t, D) \quad (8)$$

where $F_{add}(t)$ is the influx of sediment [L^2T^{-1}] supplied by longshore currents (Table 1), which can be specified for different grain-sizes (D).

$F_t(t)$ must be distributed over $F_{in,BB}$ and $F_{in,SF}$ for backbarrier and shoreface–shelf deposition before the calculation of Phases 2 and 3 can be carried out (Fig. 1).

$$F_t(t, D) = F_{in,BB} + F_{in,SF} \quad (9)$$

2.1.2. Deposition (Phases 2 and 3)

The deposition function used in the model is given by:

$$S(x, t, D) = \frac{F(x, t, D)}{h(D)} \text{ for } x \leq x_s \text{ (Phase 2)} \quad (10)$$

$$S(x, t, D) = \frac{F(x, t, D)}{h(D)} + k(t, D)$$

$$\text{for } x > x_s \text{ (Phase 3)} \quad (11)$$

where F is the flux of sediment that is in transit, available for deposition [L^2T^{-1}], h represents the sediment travel distance [L], which depends on the grain-size of the sediment and on the environment of deposition (i.e. the flow properties of the transporting medium) and k is a steady fall-out rate [LT^{-1}] of fine sediment in calm water at the shoreface–shelf (Table 1). The deposition algorithm partitions this flux of locally available sediment into a local deposition flux and a local outflux (Fig. 1):

$$F = F_{in} + F_{ero} = F_{dep} + F_{out} \quad (12)$$

However, note that F_{ero} has already been calculated in Phase 1 and therefore equals zero in Phases 2 and 3. In case of limited backbarrier accommodation $F_{out,BB} > 0$ at $x = x_m$ (calculated in Phase 2). In such case $F_{out,BB}$ is added to $F_{in,SF}$ prior to the calculation of Phase 3 in order to comply with the mass conservation principle.

The net effects of size-selective transport are simulated by the size dependence of the travel distance h in the deposition function. Cross-shore sediment dispersal is described by the following

relationship between the nominal grain diameter D [mm] and h[m], based on data from Terschelling, The Netherlands (Guillén and Hoekstra, 1996, 1997), for a standard spatial increment of 50 m as:

$$h^*(D) = c_g(x)\cdot c_w(t)\cdot\left[110 + 590\left(\frac{D_{ref}}{D}\right)^{2.5}\right] \quad \text{for } D > D_{ref} \tag{13}$$

$$h^*(D) = c_g(x)\cdot c_w(t)\cdot\left[500 + 200\left(\frac{D_{ref}}{D}\right)^{0.6}\right] \quad \text{for } D \leq D_{ref} \tag{14}$$

where $D_{ref} = 0.125$ mm. The dominant mode of transport in fully turbulent unidirectional flows of sediment below this size is in suspension, whereas sediments above this size are transported mostly as traction load (Bridge, 1981; Bridge and Bennett, 1992). Sediment transport capacity relates to wave height as waves generate offshore-directed currents during storms. However, these currents lack during fair-weather conditions. The constant $c_w(t)$ [−] accounts for this temporal variability of wave height (Table 1). The constant $c_g(x)$ [−] accounts for local conditions. This parameter has different values for deposition at shoreface–shelf and backbarrier domain.

A correction for the travel distance parameter is applied in case the spatial increment exceeds 50 m. In addition, sediment bypassing is simulated in case of subareally-exposed land to mimic washover channels. Both approaches are discussed in Storms et al. (2002).

2.2. Event-driven parameters

Large storm events are rare compared to small seasonal storms but their impact on the coastal depositional environment is larger. Most storms, both small and large, typically last a few days while fair-weather periods can last for months or years. Fig. 2 shows the wave-height distribution over a twenty-year period measured at a deep-water buoy near Schiermonnikoog, a barrier island in the northern part of The Netherlands. It shows the complete spectrum of waves, including fair-weather and storm waves. As fair-weather waves are less energetic, they are represented by the left-hand side of the graph while 'storm' waves make up the right-hand side. However, the distinction between fair-weather and storm waves is arbitrary as it depends on the time scale considered. The right-hand side of the Schiermonnikoog distribution is approximated by an expo-

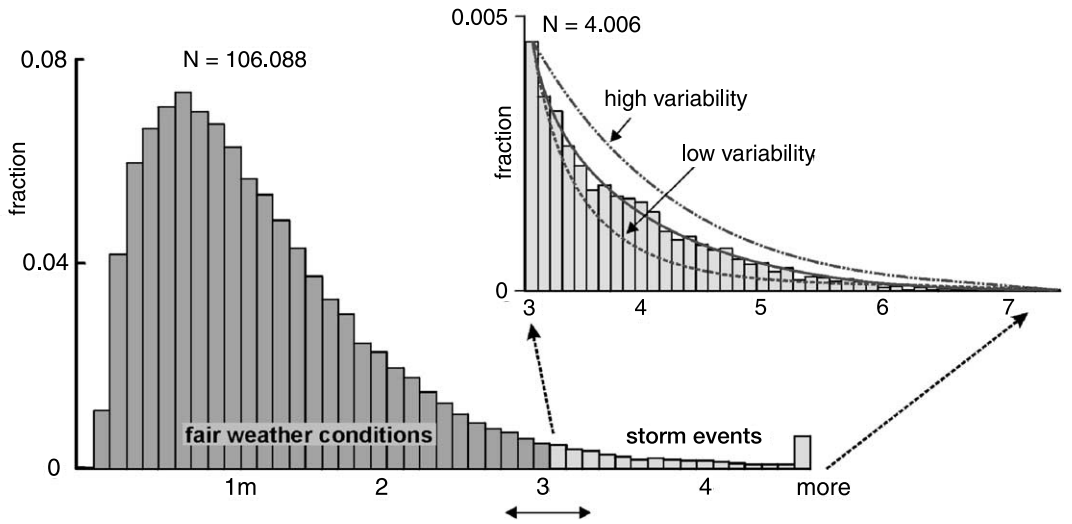

Fig. 2. Histogram showing the wave-height distribution recorded between 1997 and 1999 at a buoy (approximately 20 m water depth) near Schiermonnikoog, a barrier island in the Dutch Wadden Sea. The distinction between fair-weather and storm waves, is arbitrary fitted at 3 m in the model. Simple exponential functions are used to describe the storm wave-height distributions.

nential function, which serves to describe the wave-height regime in BARSIM (Fig. 3). Random uniform deviates R < 0,1 > are used to determine the values of $w_e(t)$:

$$w_e(t) = \frac{\ln R}{-a_1} + w_{fw} \text{ for } a_1 > 0 \quad (15)$$

where w_{fw} represents the maximum fair-weather wave height [L], which is assumed to erode smaller previously formed fair-weather scours. a_1 [−] is a constant to describe wave-height climate of different coastal settings (Table 1). The probability of a large event increases inverse proportional with constant a_1.

Fair-weather duration, Δt [T], is described as:

$$\Delta t = \frac{\ln R}{-a_2} + t_{min} \text{ for } a_2 > 0 \quad (16)$$

in which constant a_2 [−] is a measure for fair-weather duration, which is a proxy for wave-height recurrence interval (Table 1). To avoid excessive calculation times, t_{min} can be chosen to be in the order of years to decades (Table 1). A long fair-weather period, however, will embrace more small and seasonal storms than a short fair-weather period. Therefore, fair-weather wave height as used in the model is positively correlated with minimum fair-weather duration. Time-series characteristics can be changed by varying the exponential functions for both wave height and frequency distributions between or during simulations.

3. Simulated storm and fair-weather depositional patterns

Storm depositional patterns are distinctly different from fair-weather depositional patterns. At the upper shoreface, net onshore transport of sediment during fair-weather alternates with net offshore transport during storm conditions. The upper shoreface, foreshore and beach are flattened after a storm and sediment is lost to deeper water (Hobday and Reading, 1972; Reineck and Singh, 1972; Kreisa, 1981). During subsequent fair-weather conditions a steady onshore feed of sediment due to wave asymmetry enables the shoreface-beach system to recover and steepen (Lee et al., 1998).

Fig. 4 shows simulated erosion and deposition rates based on BARSIM output after storm and fair-weather conditions for a steady sea level and zero sediment supply. Absolute erosion and deposition curves during storm conditions show a wide range of values due to the variability in event

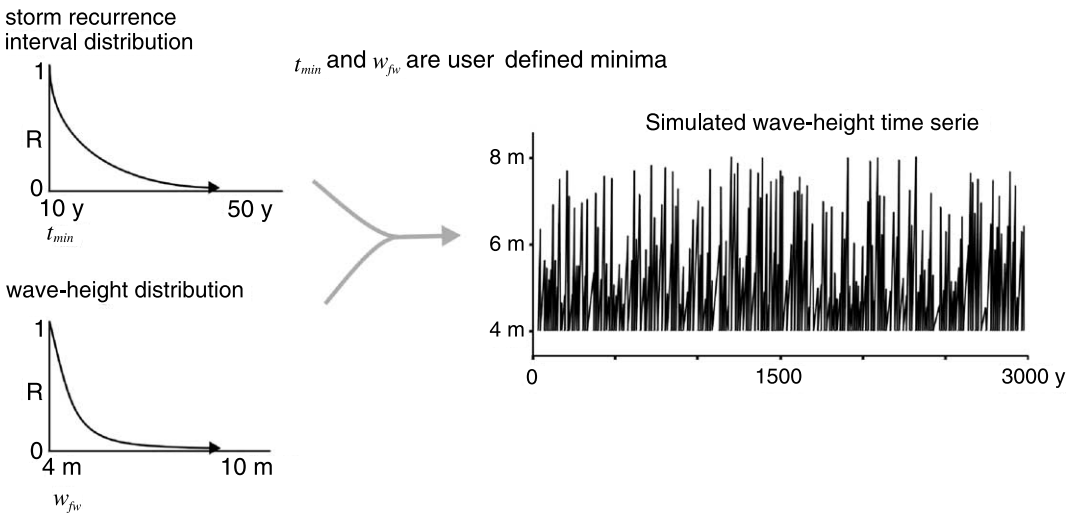

Fig. 3. Cumulative probability distributions based on exponential functions from Fig. 2 or storm wave height and recurrence interval. Independent uniform random numbers between 0 and 1 are used to draw from both distributions to create a time-series (upper right), which is used as input for BARSIM.

magnitude (Fig. 3). The maximum storm-bed thickness in this case ranges between 0.3 and 0.8 m near the shoreline and it gradually thins offshore. Storm erosion depth ranges between 0.35 and 1 m near the coastline. Fair-weather erosion and deposition values are smaller and more stable, as fair-weather 'storm' magnitude (i.e. the minor seasonal storm events that occur within a defined fair-weather period) is fixed in the model. Any variability in these curves is due to the dynamic shoreface morphology. The absolute erosion and deposition curves can be used to calculate net deposition curves that illustrate the net topographic change after either a single event or a period of fair weather (Fig. 5). As expected, simulated events cause net erosion near the coast while sediment is transported offshore (Hobday and Reading, 1972; Reineck and Singh, 1972; Kreisa, 1981). The bulk of the sediment remains fairly close to the coast (between 1 and 5 km offshore). Sediment is returned to the coast during fair-weather conditions. The overall effect after a storm–fair-weather cycle is negligible as sediment supply is zero (Fig. 5) and preservation potential of the deposits under these conditions is low because reworking provides the only source of sediment.

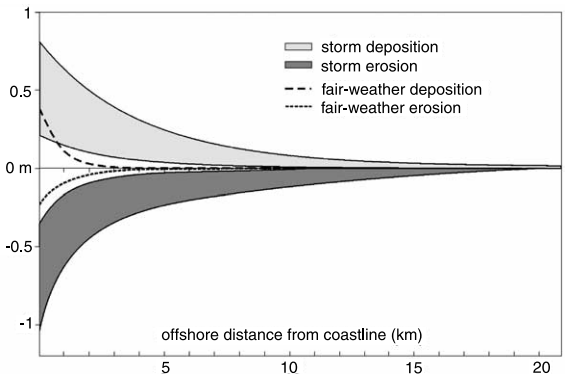

Fig. 4. Simulated absolute erosion and deposition for a steady sea level with no sediment supply. Fair-weather wave height was set to 4 m, initial substrate slope was set to 0.09°. Storm erosion and deposition are highly variable as wave height changes in time. The fair-weather duration for the simulation ranges between 10 and 53 years, on average it is nearly 16 years. Such a long fair-weather period implies that both seasonal and small events are included in the simulated fair-weather periods.

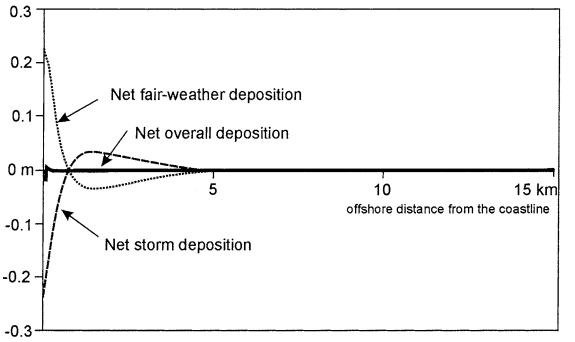

Fig. 5. Average absolute shoreface deposition for a single storm–fair-weather cycle using identical model settings as in Fig. 4. Net erosion occurs along the coastline under storm conditions as sediment is transported over a small distance in offshore direction. Sediment returns to the coastline during subsequent fair-weather conditions. The overall net result after one cycle is negligible as sediment supply is zero.

The simulated depositional patterns described above apply to a situation with a steady sea level and no sediment supply. The complexity of the depositional patterns will increase when both sea level and sediment supply vary. Therefore, in the next set of experiments (Fig. 6) sea level is held stable while sediment supply was increased to 20 m^2/yr and the fall-out rate to 0.2 mm/yr. All other model parameters are identical to the simulation described above. The simulated coastal system shows a progradational coastline. Using this setting as a base-case scenario, we tested the effects of varying wave-height regime and sediment grain-size distribution on shoreface evolution and the accompanying depositional patterns. The wave-height regime can change in time due to climatic changes (e.g. a change in prevailing wind direction or wind force). Also, a rise in sea level will change the fetch and water depth, which will affect the waves approaching the coastline.

Variation in wave-height regime (i.e. the fair-weather wave height as defined in the model) is accomplished by increasing or decreasing fair-weather wave height. This results in variation of both fair-weather and storm waves because the exponential curve used to describe storm waves is shifted along the horizontal axis of Fig. 2. The accompanying time-series for wave height will shift along the vertical axis of Fig. 3, which

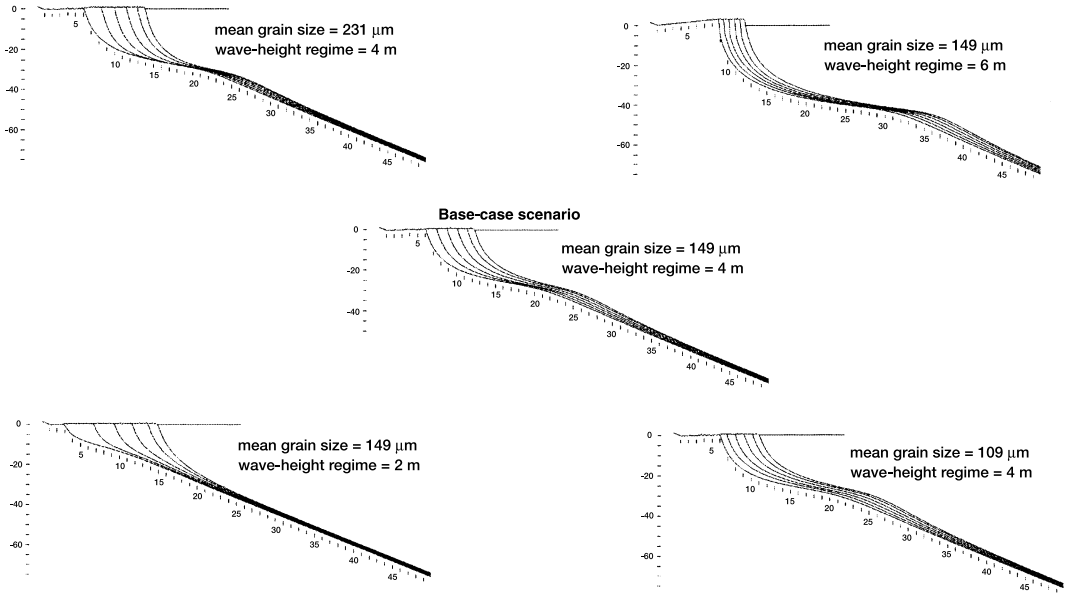

Fig. 6. Simulated timeline cross-shore plots for a 10-ky period under varying conditions of wave-height regime and grain-size of the supplied sediment. Sediment supply is 20 m^2/yr and sediment fall-out rate is 0.2 mm/yr. Wave-height regime (see text) varies from 2 to 6 m. Distinct changes in shoreface geometry can be seen as wave-height regime and grain-size are changed. Vertical scale in metres, horizontal scale in kilometres.

reflects hypothetical changes in climatic conditions through time. Wave-height regime affects both erosion and deposition in the model. Erosion will vary as the wave-base position shifts with wave height. Wave-base positions can be seen in Table 2. Deposition will be influenced, as wave-induced currents affect the sediment transport capacity. Variability in wave-height regime will therefore change the net deposition patterns as the interplay between absolute erosion and deposition rates changes. A wave-height regime of 2 m (i.e. fair-weather wave height) generates little erosive power and only a small amount of sediment is being reworked (Fig. 6). As the average wave height increases, so does the total amount of eroded sediment as both erosion depth and width of the shoreface increase. Deposition rates at the distal lower shoreface (located between the fair-weather and storm wave base; see Table 3) exceed those at the proximal lower shoreface (landward of the fair-weather wave base), which is reflected in the shoreface profile. Overall, the cross profiles shown in Fig. 6 indicate that an increase in wave-height regime leads to a steepening and widening of the shoreface in accordance with the position of the wave base.

Both sea level and climatic changes may cause variability in grain-size distribution of sediment supplied by littoral drift. A sea-level fall will force rivers to erode their own floodplain deposits thereby generating incised valleys (Zaitlin et al., 1994) and producing relatively sandy delta deposits. In time, these delta deposits will be reworked by waves and transported by longshore currents. Much of the sandy fluvial sediment load will be trapped by the infill of estuaries during a sea-level rise and only relatively fine sediment is bypassed to the marine realm. Therefore, sea-level falls may be accompanied by littoral drift adding relative fine sediment to the adjacent coastal systems. Additionally, climate will influence the overall sediment grain-size distribution of the fluvial sediment load that is supplied to the marine realm, which may therefore vary in time (Weltje et al., 1998). Consequently, it is likely that the grain-size distribution of sediment supplied by littoral drift will vary in time.

Simulations were conducted using BARSIM to

Table 2
Fair-weather wave base (FW-WB) and storm wave base (S-WB) locations (km from shoreline) for simulations described in Fig. 6

	w_{fw} = 2 m Fine	w_{fw} = 4 m Fine	w_{fw} = 6 m Fine	w_{fw} = 4 m Medium	w_{fw} = 4 m Coarse
FW-WB	4.2 ± 1.4	14.0 ± 0.5	22.5 ± 0.2	15.5 ± 0.2	11.5 ± 1.5
S-WB	9.0 ± 3.3	20.0 ± 2.6	29.2 ± 2.5	21.2 ± 2.5	18.2 ± 2.9

Wave-height regime (w_{fw}) and sediment grain-size are indicated for each simulation. Grain-size distribution is specified in Table 3.

test the effects of variations in grain-size of supplied sediment on depositional patterns and shoreface evolution. Table 3 shows the grain-size distributions used for the simulations. Grain-size does not have a direct effect on erosion in the model, because erosion is independent of sediment size (Storms et al., 2002). The shoreface will be steep (Fig. 6) if supplied sediment is coarse because coarse sediment remains close to the coast (Carter, 1988). The variability in deposition rates for the three grain-size classes differs from the pattern generated by variation in wave-height regime. The increase in shoreface slope has an indirect effect on erosion since the shoreface slope influences the wave-base location. In addition shoreface slope affects wave dissipation and therefore the erosive capacity of waves. The combination of changing erosion and deposition rates along the shoreface and shelf results in a characteristic profile of the shoreface typical for the imposed grain-size distribution.

4. Retrogradational, aggradational and progradational depositional patterns

The two examples described above illustrate how the simulated shoreface–shelf system responds to changes in wave-height regime and grain-size of supplied sediment. Both parameters impose distinct changes on depositional patterns, which are reflected in the simulated stratigraphic record. Simple geometric descriptions of the shoreface (Bruun, 1962) are no longer applicable under such conditions. Since both wave-height regime and sediment grain-size are expected to vary over geologic time scales, shallow-marine stratigraphy may well be more complex than previously considered.

Table 3
grain-size fractions of supplied sediment used during simulation runs described in Fig. 6

Grain-size class (μm)	Fine	Medium	Coarse
10	0.35	0.2	0.05
80	0.25	0.2	0.15
150	0.2	0.3	0.2
250	0.15	0.2	0.25
360	0.05	0.1	0.35
Mean (μm)	109	149	231

Simultaneous changes in sea level and sediment supply result in characteristic stratal patterns associated with regression or transgression. BARSIM was used to investigate how variations in the rate of sediment supply affect depositional patterns during three simple sea-level scenarios (falling, stable and rising sea level). Sediment supply was increased from zero to 50 m^2/yr in 5 m^2/yr increments in all three cases. Besides sediment supply, all other parameters (wave-height regime, shelf slope, sediment erodibility, fall-out rate, etc.) are identical to those of the base-case scenario described above (Fig. 6).

Fig. 7 shows the mean annual shoreface deposition rates for a steady sea level over a 10-ky period. The overall deposition rates increase as sediment supply increases. However, proximal deposition rates increase faster than distal deposition rates. As a result, progradation takes place and the shoreface steepens as more sediment is supplied. The steepening of the shoreface causes the storm and the fair-weather wave base to migrate landward (Fig. 7). Deposition rate shows a local minimum near the fair-weather wave base. Here, net erosion takes place when sediment supply rate is less than 10 m^2/yr. Variability in deposition rates due to changes in sediment supply is

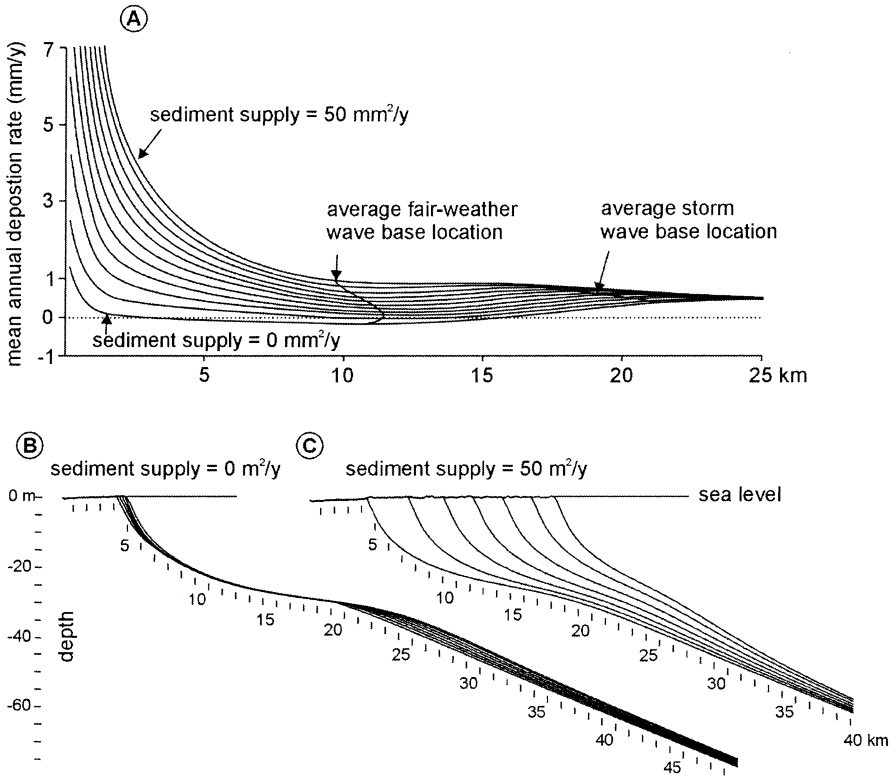

Fig. 7. (A) Simulated mean annual deposition rates for a steady sea level and sediment supply increasing from 0 to 50 m^2/yr in 5-m^2/yr increments. Fall-out rate is constant at a value of 0.2 mm/yr. The solid black lines indicate the location of the fair-weather (left) and the storm (right) wave base. Progradation rate increases with sediment supply rate. Below, two cross-shore time line plots are shown for sediment supply rates of zero (B) and 50 m^2/yr (C).

restricted to an area of about 25 km wide. Further offshore, all deposition rates will approach the sediment fall-out rate of 0.2 mm/yr.

An interesting change in depositional pattern emerges if a 1-mm/yr sea-level fall is imposed on the above scenario (Fig. 8). The middle section of the graph is pulled downward and erosion prevails while sediment supply lies between 0 and 30 m^2/yr. As the coastline progrades, erosion at the shoreface results in the formation of a regressive surface of marine erosion (Plint and Nummedal, 2000) in cases of persistent regression. This erosional surface is marked by an abrupt facies change as distal deposits are overlain by proximal deposits. The erosional surface changes into a non-depositional surface or a condensed section when the rate of sediment supply increases to 30 m^2/yr.

A sea-level rise of 1 mm/yr is imposed in the third scenario (Fig. 9). Washover deposition takes place as accommodation is created in the backbarrier during sea-level rise. This causes a decrease in sediment availability at the shoreface since washover sediment originates from the shoreface. At first, erosion takes place at the upper shoreface due to a sediment deficit. As transgression continues, net erosion in this area creates the transgressive ravinement surface (Swift, 1968). Since the volume of backbarrier deposits is restricted by backbarrier accommodation, a further increase in sediment supply will be primarily translated to an increase of shoreface sediment available to compensate proximal shoreface erosion. Retrogradation therefore gradually changes to aggradation. Deposition rate balances accommodation at a sediment supply rate of 35

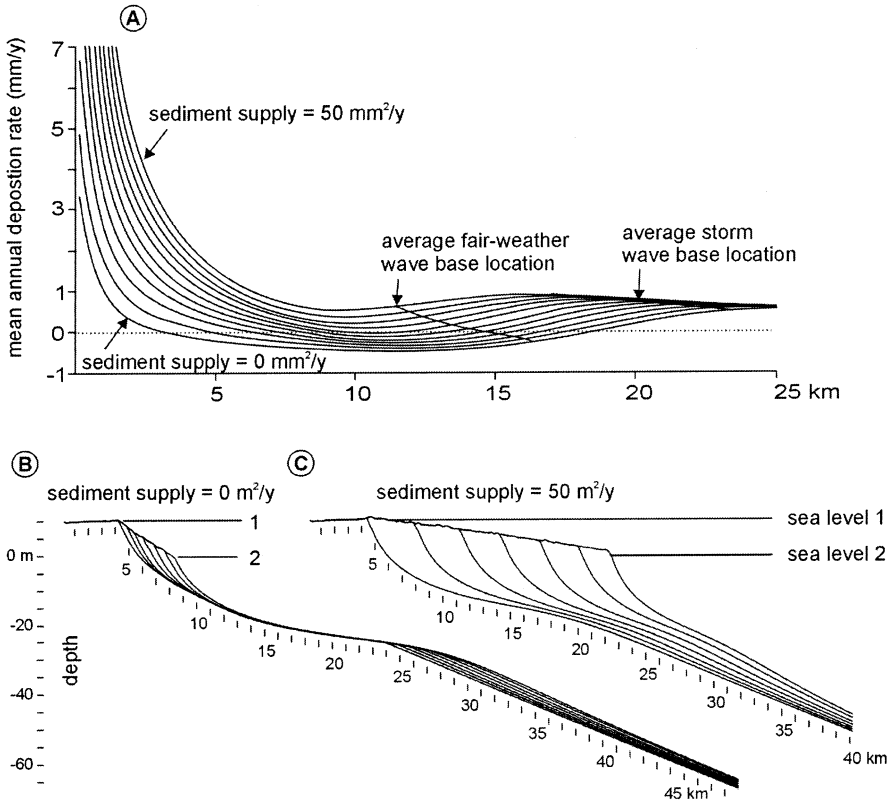

Fig. 8. (A) Simulated mean annual deposition rates for falling sea level and sediment supply increasing from 0 to 50 m^2/yr in 5-m^2/yr increments. Fall-out rate is constant at a value of 0.2 mm/yr. The solid black lines indicate the locations of the fair-weather (left) and the storm (right) wave base. Progradation rate increases with sediment supply rate. Below, two cross-shore time-line plots are shown for sediment supply rates of zero (B) and 50 m^2/yr (C). A regressive surface of marine erosion is formed in cases where sediment supply rate is 30 m^2/yr or less (B).

m^2/yr, and the coastline remains at the same position (Fig. 9). A further increase in sediment supply results in coastal progradation and the mean annual deposition rates are comparable to patterns seen in Figs. 7 and 8.

The cross-shore variability in net deposition rates described above contradicts the intuitive notion that deposition rate should decrease gradually in a seaward direction. They explain both the presence and the absence of specific shoreface deposits. During a forced regression with a low supply of sediment (Fig. 8), upper shoreface deposits overlie lower shoreface and shelf deposits. In such cases middle shoreface deposits are replaced by an erosional or a non-depositional surface.

5. Simulated event stratigraphy

Up to this point, BARSIM model output described dynamic features of coastal systems that cannot be compared to real-world data. However, BARSIM can also produce output in formats that more closely resemble sedimentological data, which are easier to evaluate and interpret. Mean annual deposition rates explain the general behaviour of coastal systems over geologic time scales, and illustrate the coastal response to variations in sea level, sediment supply, wave-height regime and grain-size. In reality, strata that originate from individual events show a high degree of complexity which effectively conceals these aver-

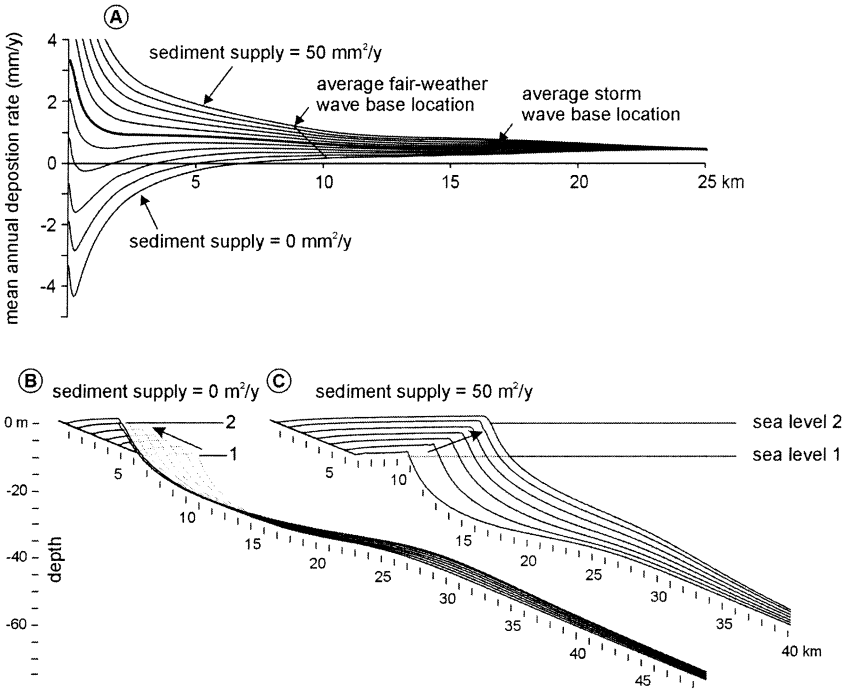

Fig. 9. (A) Simulated mean annual deposition rates for a rising sea level and sediment supply increasing from 0 to 50 m^2/yr in 5-m^2/yr increments. Fall-out rate is constant at a value of 0.2 mm/yr. The solid black lines indicate the location of the fair-weather (left) and the storm (right) wave base. Initial retrogradation and formation of transgressive erosion surface (B) changes to progradation (C) as sediment supply increases (see arrows).

age deposition rates. Little is known about the completeness of individual event beds, and even less about the relation between their measurable characteristics (grain-size and thickness) and formative mechanisms. It will be shown below that patterns emerge in simulated bed successions, which tell us more about the positioning (cf. water depth) at the shoreface during deposition. These patterns may help us to recognise specific changes in depositional pattern along the shoreface shelf system that can be attributed to variability in sea level, sediment supply, wave-height regime and grain-size change.

A simple progradational system was simulated during a 15-ky period to evaluate bed variability along the shoreface–shelf system. During this simulation sea level remained constant and the rate of sediment supply was fixed at 20 m^2/yr, while

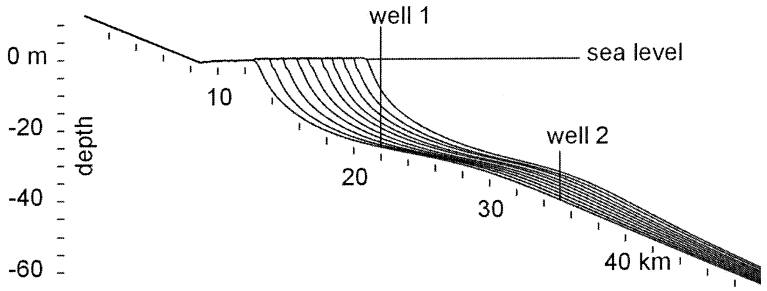

Fig. 10. Simulated cross-shore time line profile for a 15-ky simulation with steady sea level and 20 m^2/yr. Fall-out rate remains at 0.2 mm/yr. Two wells, located at the shoreface, are discussed in Fig. 11.

fall-out rate was set to 0.2 mm/yr. The coastline prograded about 8 km during the 15-ky interval (Fig. 10). Bed thickness, grain-size and type of bed (storm vs. fair weather), as well as water depth at the time of deposition were recorded in 37 wells located at 1-km intervals along the shoreface. Two wells located at km 22 and 35 are shown in detail (Figs. 11 and 12). Well 1 (Fig. 11) is located landward of the fair-weather wave base. The sediments in this well consist only of event beds with an overall coarsening upward trend. Water depth during deposition (see scale bar) gradually decreases from 26 to 8 m. Well 2 (Fig. 10) shows deposits located further offshore. Water depth during deposition ranges between 32 and 40 m, which coincides with the most frequent position of the storm wave base (Fig. 13). Some sediments were deposited seaward of the wave base while other sediments were deposited landward of the wave base. Fair-weather beds are preserved if subsequent storms are mild. A detailed view of Well 2 reveals that the mean grain-size of fair-weather beds is 10 to 15 microns, which allows them to be interpreted as fall-out deposits.

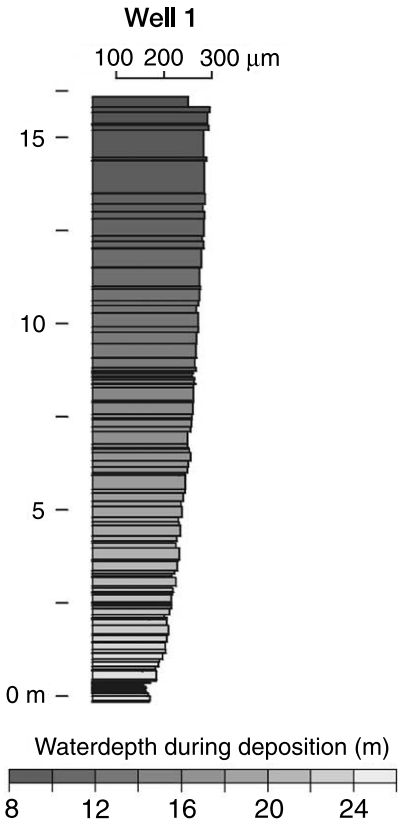

Fig. 11. Simulated Well 1 (see Fig. 10 for location) illustrating the mean grain-size and water depth during deposition. The well shows an overall coarsening upward trend as well as a thickening upward trend of beds. Water depth decreased from 26 to 8 m as the coastline prograded. All beds are formed under storm conditions.

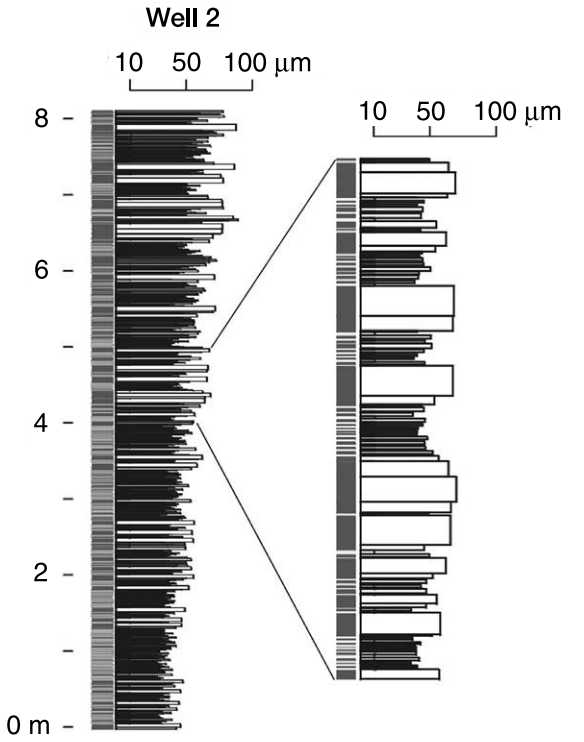

Fig. 12. Simulated Well 2 (see Fig. 10 for location) illustrating the mean grain-size and water depth during deposition. The column left of the well indicates whether the bed was formed under storm (black) or fair-weather conditions (white). Water depth decreased from 40 to 31 m as the coastline prograded during deposition. The enlarged part shows a 1-m interval with considerable grain-size and bed-thickness variability.

Fig. 14 shows four plots that illustrate different bed characteristics vs. water depth during deposition based on all preserved fair-weather and storm beds. Average bed thickness decreases in an offshore direction (Fig. 14A). The standard deviation of bed thickness is equivalent to the mean value indicating a large variability. Niedo-

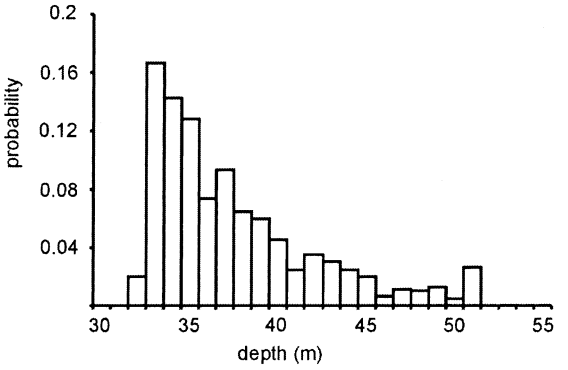

Fig. 13. Histogram showing the storm wave-base water depth during the simulation described above. Average storm wave-base water depth is 37 m, while the minima and maxima range between 32 and 52 m.

roda et al. (1989) found similar results for bed variability and mean bed thickness. The mean grain-size of the beds decreases in an offshore direction (Fig. 14B), while the standard deviation reaches a maximum near water depths of 25–30 m, which coincide with the fair-weather wave base location. Fig. 14C shows that essentially all beds deposited in water depths between 10 and 30 m are storm beds and thus consist solely of reworked sediment. The relatively low standard deviation of grain-size in these shallow waters indicates that deposition of reworked storm beds is an efficient sorting mechanism. The origin of very thin beds is difficult to determine from logs or cores. Therefore, the measured ratio between storm and fair-weather beds is affected by the ability to recognise them in the stratal record. To simulate the limited resolution of real-world data, a constraint is imposed in the model through the use of a minimum event-bed thickness of either 2 or 5 mm (Fig. 14C). If an event bed is too thin it amalgamates with fair-weather deposits to form a heterogeneous background deposit. Fair-weather bed preservation potential increases with water depth as erosion capacity decreases (Fig. 14C). An increase of the minimum event-bed thickness in the model leads to a de-

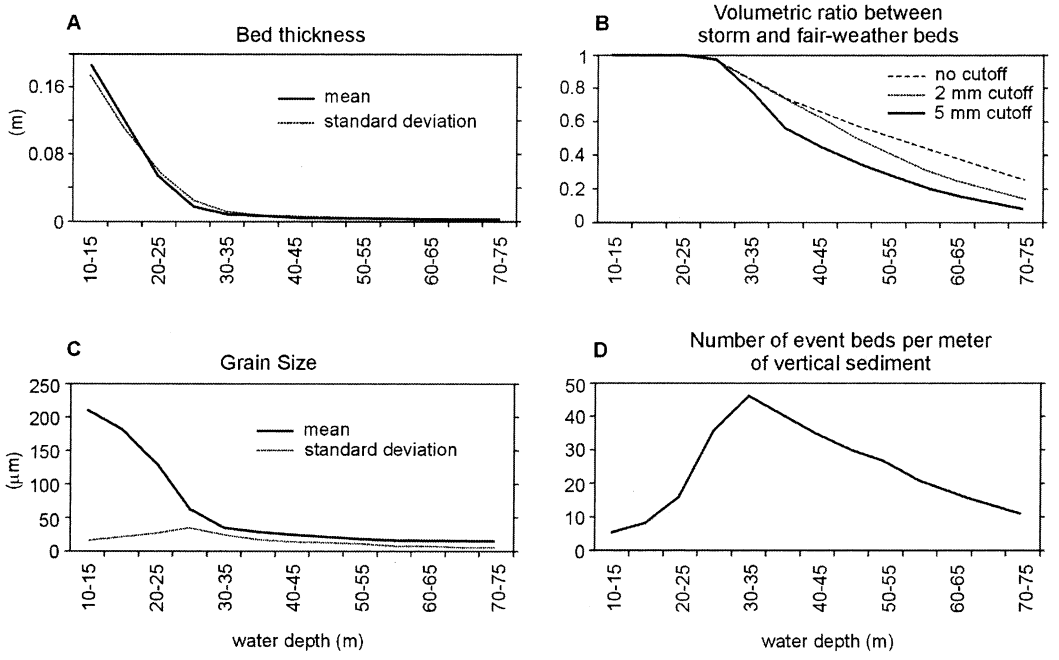

Fig. 14. Plots showing bed characteristics based on 37 simulated wells positioned along the shoreface and shelf (see Fig. 10) between km 34 and 58 with 1-km intervals. Well 1 and 2 are also included in this simulated data set. (A) Cross-shore variation of mean bed thickness and standard deviation. (B) Cross-shore variation of mean grain-size and standard deviation. (C) Cross-shore ratio between event and fair-weather beds. (D) Absolute number of event beds per metre of vertical sediment.

crease in the number of event beds, which affects the storm–fair-weather bed ratio (Fig. 14C). The absolute number of recognisable event beds (>5 mm) per metre of vertical sediment column (Fig. 14D) shows a distinct peak near 30–35 m water depth. Landward of this point, the absolute number of beds depends on the bed thickness (Fig. 14A). A decrease in the absolute number of event beds caused by starvation as water depth increases is observed seaward of the peak. A water depth of 30–35 m corresponds to a distance to 10 km to the shoreline (Fig. 10). Zhang et al. (1997) found a similar peak in bed rhythmicity at the same distance from the coastline using both numerical simulations and box core data of the Northern California shelf.

6. Discussion and conclusions

6.1. Model resolution

The definition of a minimum duration for fair-weather conditions provides a way to change the temporal resolution of the model. All examples discussed above used a minimum fair-weather time step of 10 years in order to simulate geologic time scales. Model resolution in this case is fairly low, but simulated bed characteristics (Fig. 14) show trends comparable to those of field studies (Reineck and Singh, 1972; Aigner, 1985; Snedden and Nummedal, 1991). By reducing the minimum duration for fair-weather conditions to days, it becomes possible to simulate each individual windy or stormy occurrence. In that case, fair-weather wave height should be low and wave-height variability should be high. In fact, modelling with time steps of the order of one day may help to reconstruct palaeo-wave-height climate from specific sections of the stratigraphic record.

6.2. Bedforms

The presence of crossbedding caused by ripple and dune formation in upper shoreface deposits leads to variability in bed thickness over short distances. Further seaward, crossbedding is replaced by parallel lamination as flow velocity decreases. Beds become more continuous and predictable. Therefore, modelled beds should not be used for interpretations in water depths of less than 10 m, to avoid bedform deviations. Mechanisms of bed destruction that are not included in the model are coast parallel currents (either storm or tide driven), which may form bars at greater depths, and biological activity at the shoreface and shelf. The bars may limit the lateral continuity of event beds (Cacchione et al., 1984) while bioturbation may lead to mixing of the upper 10 cm (Wheatcroft, 1990; Wiberg, 2000). The presence of bedforms and bioturbation does not affect the simulated coastal response, because the net deposition rate is not affected by their presence or absence.

6.3. Definition of facies

The simulation of a regressive shoreface–shelf system (Figs. 11–13) shows that water depth alone is insufficient to define facies, because it decreases gradually during deposition. Wells 1 and 2 (Figs. 11 and 12) show that different types of deposits emerge which can be classified according to the lithofacies scheme proposed by Swift et al. (1991) which is based on three types of lithofacies: amalgamated sand facies, interstratified sand and mud facies, and laminated mud facies. The boundary between the amalgamated sand facies and the interstratified sand and mud facies can easily be established based on the presence of mud interbeds. However, the boundary between the interstratified mud and sand facies and the laminated mud facies is diffuse and arbitrary. Fig. 15 illustrates mean facies grain-size and variability of 0.5-m sediment intervals based on the simulated shoreface–shelf sediments described above (Fig. 10). Three populations can be recognised that agree well with the facies scheme proposed by Swift et al. (1991). The high reworking efficiency of the upper and middle shoreface (landward of the fair-weather wave base) reduces the preservation potential of fine-grained fair-weather beds zero (Fig. 14C) so that all sand beds are amalgamated. Variability in grain-size is therefore low. Further seaward, fine-grained fair-weather beds are more likely to be preserved,

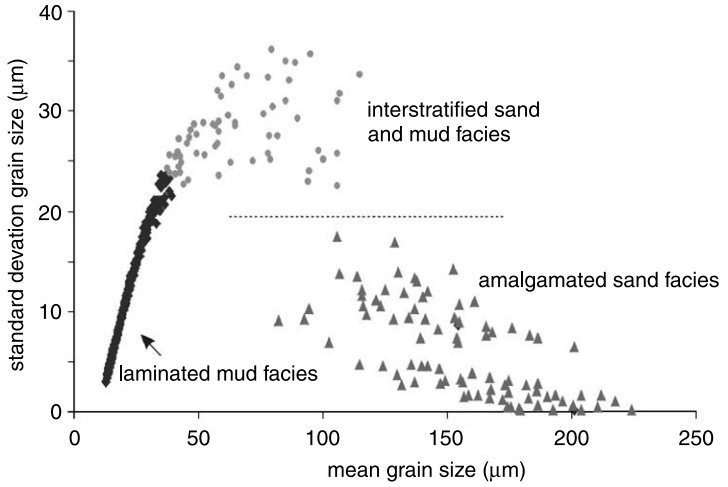

Fig. 15. Facies definition based on the mean and standard deviation of simulated sediment grain-size, using data from the simulated progradational sequence shown in Fig. 10. Three populations can be recognised that support the facies scheme proposed by Swift et al. (1991). Amalgamated sand facies are characterised by a high mean grain-size and a relative low standard deviation. The interstratified sand and mud facies show a sharp decrease in mean grain-size while the standard deviation rapidly increases. Laminated mud facies is characterised by a low mean and standard deviation of the grain-size.

leading to the formation of interstratified sand and mud facies. Here, the presence of fine-grained beds between sandy beds causes an increase of the grain-size variability within the 0.5-m sediment intervals while the mean grain-size decreases. As the sand content decreases in offshore direction due to starvation, laminated mud facies form which are characterised by a decrease in mean and standard deviation of the grain-size. Based on the classification shown in Fig. 15 it is concluded that Well 1 (Fig. 11) consists of amalgamated sand facies, while Well 2 (Fig. 12) consists of laminated mud facies. In contrast to grain-size, no clear relation was found between mean and variation in bed thickness which could help identify facies type.

6.4. Conclusions

BARSIM is a model that bridges the gap between micro (i.e. civil engineering) and macro (i.e. basin fill) scale modelling. By using event deposition as a basis for modelling, both small-scale variability and large-scale coastal behaviour can be explained which eliminates the need to model different processes over different time scales. The storm wave base location is of key importance in the model as it defines the outer limit of erosion which affects both average deposition patterns as well as the preservation potential of individual beds. Shoreface depositional patterns show a large variability in average deposition rate under conditions of varying sea level, sediment supply, wave-height and grain-size. Changes in the rates of sea-level change and sediment supply traditionally are considered to be the main mechanisms for generating the observed stratal variability in shallow-marine settings. However, model results indicate that less obvious variables such as wave-height regime and grain-size of the supplied sediment have equally significant effects on stratal geometry. Unravelling coastal evolution from the shallow-marine stratigraphic record may be more difficult than previously assumed, as these variables are expected to vary over geologic time scales.

Acknowledgements

This research was financed by the Delft Interfacultary Research Centre (DUT-DIOC 3.3) of the Delft University of Technology. I would like to thank Gert Jan Weltje, Irina Overeem, Kees

Geel, Donald Swift, Shejun Fan, and Gary Hampson for their discussions while constructing and testing the event deposition model. Careful reading by Gert Jan Weltje and Salomon Kroonenberg as well as *Marine Geology* reviewers James Syvitski and Peter Cowell considerably improved the manuscript.

References

Aigner, T., 1985. Storm Depositional Systems. Lecture Notes in Earth Sciences, vol. 3, Springer, Berlin, 174 pp.

Battacharyya, A., Sarkar, S., Chanda, S.K., 1980. Storm deposits in the late Proterozoic lower Bhander sandstone of Vindhyan supergroup around Miahar, Satna district, Madhya Pradesh, India. J. Sediment. Petrol. 50, 1327–1336.

Bridge, J.S., 1981. Hydraulic interpretation of grain-size distributions using a physical model for bedload transport. J. Sediment. Petrol. 51, 1109–1124.

Bridge, J.S., Bennet, S.J., 1992. A model for entrainment and transport of sediment grains of mixed sizes, shapes and densities. Water Resources Res. 28, 337–363.

Bruun, P., 1962. Sea level rise as a cause of shore erosion. Am. Soc. Civil Eng. Proc., J. Waterw. Harb. Div. 88, 117–130.

Cookman, J.L., Flemmings, P.B., 2001. STORMSED1.0: Hydrodynamics and sediment transport in a 2D steady state. Comput. Geosci. 27, 647–675.

Cacchione, D.A., Drake, D.E., Grant, W.D., Tate, G.B., 1984. Rippled scour depressions of the inner continental shelf of central California. J. Sediment. Petrol. 54, 1280–1291.

Carey, J.S., Swift, D.J.P., Steckler, M., Reed, C.R., Niedoroda, A.W., 1999. High-resolution sequence stratigraphic modeling 2: Effects of sedimentation processes. In: Harbaugh, J.W, Watney, W.L., Rankey, E.C., Slingerland, R., Goldstein, R.H., Franseen, E.K. (Eds.), Numerical Experiments in Stratigraphy: Recent Advances in Stratigraphic and Sedimentologic Computer Simulations. SEPM, Spec. Publ. 62, pp. 151–164.

Carter, R.W.G., 1988. Coastal Environments – An Introduction to the Physical, Ecological and Cultural Systems of Coastlines. Academic Press, London, 617 pp.

Cowell, P.J., Roy, P.S., Cleveringa, J., De Boer, P.L., 1999a. Simulating coastal systems tracts using the shoreface translation model. In: Harbaugh, J.W, Watney, W.L., Rankey, E.C., Slingerland, R., Goldstein, R.H., Franseen, E.K. (Eds.), Numerical Experiments in Stratigraphy: Recent Advances in Stratigraphic and Sedimentologic Computer Simulations. SEPM, Spec. Publ. 62, pp. 165–175.

Cowell, P.J., Hanslow, D.J., Meleo, J.F., 1999b. The shoreface. In: Short, A.D. (Ed.), Handbook of Beach and Shoreface Morphodynamics. Wiley, New York, 379 pp.

Crowley, K.D., 1984. Filtering of depositional events and the completeness of sedimentary cycles. J. Sediment. Petrol. 54, 127–136.

Dott, R.H., Jr., 1983. 1982 SEPM Presidential Address: Episodic sedimentation – how normal is average? How rare is rare? Does it matter? J. Sediment. Petrol. 53, 5–23.

Drake, D.E., 1999. Temporal and spatial variability of the sediment grain-size distribution on the Eel shelf: The flood layer of 1995. Mar. Geol. 154, 169–182.

Field, M.E., Roy, P.S., 1984. Offshore transport and sandbody formation: Evidence from a steep, high-energy shoreface, southeastern Australia. J. Sediment. Petrol. 54, 1292–1302.

Gretener, P.E., 1967. Significance of the rare event in geology. Am. Assoc. Pet. Geol. Bull. 51, 2197–2206.

Guillén, J., Hoekstra, P., 1996. The 'equilibrium' distribution of grain-size fractions and its implications for cross-shore sediment transport: A conceptual model. Mar. Geol. 135, 15–33.

Guillén, J., Hoekstra, P., 1997. Sediment distribution in the near shore zone: Grain-size evolution in response to shoreface nourishment (Island of Terschelling, The Netherlands). Estuar. Coast. Shelf Sci. 45, 639–652.

Harris, C.K., Wiberg, P.L., 2001. A two-dimensional, time-dependent model of suspended sediment transport and bed reworking for continental shelves. Comput. Geosci. 27, 675–690.

Hobday, D.K., Reading, H.G., 1972. Fair weather versus storm processes in shallow marine sand bar sequences in the late Precambrian of Finnmark, North Norway. J. Sediment. Petrol. 42, 318–324.

Kreisa, R.D., 1981. Storm-generated sedimentary structures in subtidal marine facies with examples from the middle and upper Ordovician of southwestern Virginia. J. Sediment. Petrol. 51, 823–848.

Kumar, N., Sanders, J.E., 1976. Characteristics of shoreface storm deposits: Modern and ancient examples. J. Sediment. Petrol. 46, 145–162.

Lavelle, J.W., Swift, D.J.P., Gadd, P.E., Stubblefield, W.L., Case, F.N., Brashear, H.R., Haff, K.W., 1978. Fair weather and storm sand transport on the Long Island, New York, inner shelf. Sedimentology 25, 823–842.

Lee, G., Nicholls, R.J., Birkemeier, W.A., 1998. Storm-driven variability of the nearshore-profile at Duck, North Carolina, USA, 1981–1991. Mar. Geol. 148, 163–177.

Li, M.Z., Amos, C.L., 2001. SEDTRANS96: The upgraded and better calibrated sediment-transport model for continental shelves. Comput. Geosci. 27, 619–646.

Madsen, O.S., 1991. Mechanics of cohesionless sediment transport in coastal waters. Proc. Coastal Sediments 1991, ASCE, New York, pp. 15–27.

Myrow, P.M., Southard, J.B., 1996. Tempestite deposition. J. Sediment. Res. 66, 875–887.

Niedoroda, A.W., Swift, D.J.P., Hopkins, T.S., Ma, C., 1984. Shoreface morphodynamics on wave-dominated coasts. Mar. Geol. 60, 331–354.

Niedoroda, A.W., Swift, D.J.P., Thorne, J.A., 1989. Modeling shelf storm beds: Controls of bed thickness and bedding sequences. In: Morton, R.A., Nummedal, D. (Eds.), Shelf Sedimentation, Shelf Sequence and Related Hydrocarbon

Accumulation. Gulf Coast Section, 7th Annual Research Conference Proceedings, SEPM, pp. 15–39.
Niedoroda, A.W., Reed, C.W., Swift, D.J.P., Arato, H., Hoyanagi, K., 1995. Modeling shore-normal large-scale coastal evolution. Mar. Geol. 126, 181–199.
Paola, C., 2000. Quantitative models of sedimentary basin filling. Sedimentology 47, 121–178.
Plint, A.G., Nummedal, D., 2000. The falling stage systems tract: Recognition and importance in sequence stratigraphic analysis. In: Hunt, D., Gawthorpe, R.L. (Eds.), Sedimentary Responses to Forced Regressions. Geol. Soc. Spec. Publ. 172, pp. 1–17.
Reineck, H.E., Singh, I.B., 1972. Genesis of laminated sand and graded rhythmites in storm-sand layers of shelf mud. Sedimentology 18, 123–128.
Sadler, P.M., 1981. Sediment accumulation rates and the completeness of stratigraphic sections. J. Geol. 89, 569–584.
Schwarzacher, W., 2000. Repetitions and cycles in stratigraphy. Earth-Sci. Rev. 50, 51–75.
Snedden, J.W., Nummedal, D., Amos, A.F., 1988. Storm and fair-weather combined flow on the central Texas continental shelf. J. Sediment. Petrol. 58, 580–595.
Snedden, J.W., Nummedal, D., 1991. Origin and geometry of storm-deposited sand beds in the modern sediments of the Texas continental shelf. In: Swift, D.J.P., Oertel, G.F., Tillman, R.W., Thorne, J.A. (Eds.), Shelf Sand and Sandstone Bodies. Int. Assoc. Sedimentol. Spec. Publ. 14, pp. 283–308.
Steckler, M., 1999. High-resolution sequence stratigraphic modeling 1: The interplay of sedimentation, erosion, and subsidence, In: Harbaugh, J.W, Watney, W.L., Rankey, E.C., Slingerland, R., Goldstein, R.H., Franseen, E.K. (Eds.), Numerical Experiments in Stratigraphy: Recent Advances in Stratigraphic and Sedimentologic Computer Simulations. SEPM, Spec. Publ. 62, pp. 139–149.
Storms, J.E.A., Weltje, G.J., van Dijke, J.J., Geel, C.R., Kroonenberg, S.B., 2002. Process-response modeling of wave-dominated coastal systems: Simulating evolution and stratigraphy on geological timescales. J. Sediment. Res. 72, 226–239.
Swift, D.J.P., 1968. Coastal erosion and transgressive stratigraphy. J. Geol. 76, 444–456.
Swift, D.J.P., Phillips, S., Thorne, J.A., 1991. Sedimentation on continental margins, IV. Lithofacies and depositional systems. In: Swift, D.J.P., Oertel, G.F., Tillman, R.W., Thorne, J.A. (Eds.), Shelf Sand and Sandstone Bodies. Int. Assoc. Sedimentol. Spec. Publ. 14, pp. 89–152.
Syvitski, J.P.M., Hutton, E.W.H., 2001. 2D SEDFLUX 1.0C: An advanced process-response numerical model for the fill of marine sedimentary basins. Comput. Geosci. 27, 731–753.
Thorne, J.A., Swift, D.J.P., 1991. Sedimentation on continental margins, II. Application of the regime concept. In: Swift, D.J.P., Oertel, G.F., Tillman, R.W., Thorne, J.A (Eds.), Shelf Sand and Sandstone Bodies. Int. Assoc. Sedimentol. Spec. Publ.n 14, pp. 33–58.
Tipper, J.C., 2000. Patterns of stratigraphic cyclicity. J. Sediment. Res. 70, 1262–1279.
Weltje, G.J., Meijer, X.D., De Boer, P.L., 1998. Stratigraphic inversion of siliciclastic basin fills: A note on the distinction between supply signals resulting from tectonic and climatic forcing. Basin Res. 10, 129–153.
Wheatcroft, R.A., 1990. Preservation potential of sedimentary event layers. Geology 18, 843–845.
Wiberg, P., 2000. A perfect storm: Formation and potential for preservation of storm beds on the continental shelf. Oceanography 13, 93–99.
Zaitlin, B.A., Dalrymple, R.W., Boyd, R., 1994. The stratigraphic organization of incised valley systems associated with relative sea-level change. In: Dalrymple, R.W., Boyd, R., Zaitlin, B.A. (Eds.), Incised Valley Systems: Origin and Sedimentary Sequences. Soc. Econ. Paleontol. Mineral. Spec. Publ. 51, pp. 45–60.
Zhang, Y., Swift, D.J.P., Niedoroda, A.W., Reed, C.W., Thorne, J.A., 1997. Simulation of sedimentary facies on the northern California shelf. Geology 25, 635–638.
Zhang, Y., Swift, D.J.P., Fan, S., Niedoroda, A.W., Reed, C.W., 1999. Two-dimensional numerical modeling of storm deposition on the northern Californian shelf. Mar. Geol. 154, 155–167.